15th Australasian Fluid Mechanics Conference
The University of Sydney, Sydney, Australia
13-17 December 2004

Hydrodynamic Performance of a Surfboard Fin

P.A. Brandner[1] and G.J. Walker[2]

[1]Faculty of Maritime Transport and Engineering
Australian Maritime College, Launceston Tasmania, 7248 AUSTRALIA

[2]School of Engineering
University of Tasmania, Hobart, Tasmania, 7001 AUSTRALIA

Abstract

The performance of a generic surfboard fin is investigated in a cavitation tunnel to gain basic understanding of the viscous flows involved for future systematic experimental and computational studies. Measurements of lift and drag forces, pitching moment and results of flow visualisation are presented. Surface flow visualisation studies reveal relatively complex boundary layer transition and separation phenomena although lift and drag characteristics are virtually invariant with Reynolds number in the range tested. A mixed two- and three-dimensional separation behaviour is observed at high incidence.

Introduction

Increasing competition and professionalism in the sport of wave surfing has created an increasing desire to improve equipment performance. A project is underway at the Australian Maritime College (AMC) to investigate the performance of surfboard fins. The board's fins provide the basis for control and manoeuvrability and for the purposes of this study involve the three-fin configuration typical of modern surfboards – as shown in Figure 1. These consist of two cambered side fins and one symmetric centre fin. The side fins are located near the edge of the surfboard at approximately 80% of the board length from the nose and the centre fin is located on the centreline at approximately 90% of the board length from the nose. The side fins are canted outward at approximately 5 to 10° to maintain verticality in a turn whilst the centre fin is upright. The side fins are also toed in approximately 4 to 8° to achieve zero lift incidence for linear motion. Lift (or side force for manoeuvring of the surfboard) is produced by the combined effects of the centre fin and the fin on the inner side of the turn. However the side fins, being cambered, produce most of the lift and are the subject of the present investigation. They are typically of intermediate to low aspect ratio and have a moderately swept planform [5]. Foils typically have a thickness to chord ratio of approximately 10% with an arbitrarily curved low-pressure surface and a flat high-pressure surface. The leading edges usually have a relatively small radius.

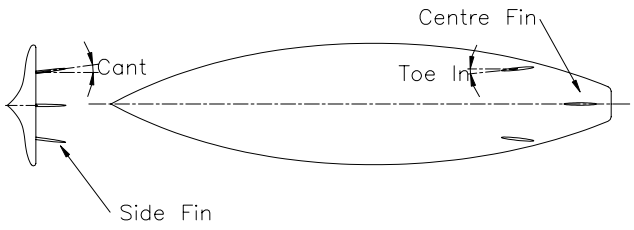

Figure 1. Typical Modern Surfboard Fin Arrangement.

There is currently no definitive information available on surfboard relative speeds and fin incidences and their dependence on wave size. In the absence of this data it is estimated that speeds may reach 10 to 15 m/s. Typical fin chords are of the order of 0.1m giving typical chord based Reynolds numbers, (R_n) between 10^5 to 10^6. This is a range where transitional flow and separation effects are known to be significant. Given the range and type of manoeuvres performed with surfboards it can be expected that the fins would operate over a wide range of incidence including stall. Preliminary testing on production fins has shown that a range of viscous flow effects may occur including leading and trailing edge separation, laminar separation and laminar bubble bursting. Testing has also shown that significant cavitation phenomena may occur, but this is beyond the scope of the present paper.

Fins designs have to date been based on practical experience of surfboard and accessory manufacturers with significant emphasis on aesthetic considerations and perceived market expectations. Whilst there exists considerable published data on the performance of foil sections and lifting surfaces [5] and some specific studies [4] a literature survey has revealed little information on the performance of lifting devices with this range of flow parameters and geometry. There is therefore considerable scope for characterising viscous and cavitating flows on surfboard fins and identifying how these are affected by foil geometry. The ultimate objective of this work is to optimise fin designs for various Reynolds numbers and incidences. The aim of the present investigation is to characterise performance of a lifting surface typical of a surfboard side fin and to gather data that may form the basis of more detailed investigation and optimisation using experiment and CFD. Observations made include measurements of lift and drag forces, pitching moments and on- and off-body flow visualisation for characterisation of viscous flows.

Experimental Overview

Surfboard Fin Geometry

A simple geometry representative of typical surfboard fins was chosen for the present study. The test foil has an elliptical planform and a NACA 4 digit half section with a flat pressure surface. The fin is swept by offsetting the 65% chord position on a 25° inclined generator line. Geometric parameters are summarised in Table 1. The fin was manufactured using numerically controlled machining from commercially available fibre reinforced plastic sheet and coated with a black coloured epoxy for contrast in flow visualisation tests.

Span, S	0.12m
Base Chord, c	0.1m
Planform Area, A	0.00962m^2
Sweep angle, Λ	25°
Planform	Elliptical
Aspect ratio, AR	3
Thickness/Chord, t/c	9% (constant)
Section	Half NACA 0009
Leading edge radius	0.5% of c

Table 1. Summary of Surfboard Fin Geometric Parameters.

Cavitation Tunnel Experimental Set Up

All tests where performed in the Tom Fink Cavitation Tunnel, a closed recirculating variable pressure water tunnel. The test section dimensions are 0.6m x 0.6m cross section x 2.6m long. The velocity may be varied from 2 to 12m/s and the centreline static pressure from 4 to 400 kPa absolute. Studies may involve the investigation of steady and unsteady flows, two-phase flows including cavitation, turbulence and hydro-acoustics. Full details of the tunnel and its capabilities are given by Brandner and Walker [2].

The fin was mounted on a 0.16m diameter flush penetration on the ceiling of the test section 1.15m from the entrance to achieve a similar boundary layer thickness to that on a surfboard. Typical surfboard lengths are 1.5m and for the expected Reynolds Number range a turbulent flat plate boundary layer thicknesses would be of the order of 0.02m assuming a $1/7^{th}$ power law. This gives a boundary layer thickness/fin span ratio of 1/6.

Parameters measured during testing include tunnel pressure, velocity, temperature and dissolved oxygen content. Online instrumentation is used for automatic control of tunnel pressure and velocity as well as real time data monitoring and acquisition. The test section pressure is measured using 2 *Rosemount* Model 3051C Smart absolute pressure transducers in parallel. Test section velocity is derived from the contraction pressure differential measured using 2 *Rosemount* Model 1151 Smart differential pressure transducers in parallel. One of each pressure transducer pair has a lower range to improve measurement precision at lower pressures and velocities respectively. The estimated precision of the absolute pressure measurement is 0.1 kPa for pressures up to 120 kPa and 0.5 kPa for pressures up to 400 kPa. The estimated precision of the velocity measurement is 0.05 m/s. Water temperature is measured to 0.5°C accuracy using a *Rosemount* Model 244 temperature transducer. Dissolved Oxygen content is measured using a *Rosemount* Model 499 Dissolved Oxygen sensor. Pitot tube pressures relative to the tunnel static pressure (as well as tunnel instrument pressures) were measured sequentially using a *Validyne* Model DP15TL differential pressure transducer via a Model 48J7-1 *Scanivalve* pressure multiplexer.

Measurements of tunnel wall boundary layer profiles were made using a 1.6mm diameter Pitot tube, a wall static tapping and an automated traverse. The velocity profiles closely follow those of the standard law of the wall for turbulent flow. Measurements of lift, drag and pitching moment acting on the fin were performed using a six-component force balance developed at the AMC [1]. Balance calibration data indicates a precision of 0.13 N for the three force components and 0.03Nm for the three moment components. The fin incidence was set using the balance to an estimated absolute precision of 0.05°. For the flow visualisation studies the incidence of the model could be set with an estimated precision of 0.25°.

Experimental Procedure

The following tests were performed:
(i) Measurement of lift and drag forces and pitching moment;
(ii) On body flow visualisation using oil flow tests;
(iii) Off body flow visualisation using air injection.

Measurements of lift, drag and pitching moment were made at incidence angles, α, varying between -6 to 26° in increments of 1° and Reynolds Numbers between $2x10^5$ to 10^6 in increments of $2x10^5$. Reynolds Number is defined by $R_n = Uc/\nu$ where U is the freestream velocity, c the fin base chord and ν the kinematic viscosity. To investigate hysteresis effects measurements were made with both increasing and decreasing incidence for all Reynolds numbers tested. The force balance is calibrated as a six-component linear instrument resulting in a 36 coefficient calibration matrix. A circular penetration for model mounting is used for connecting the model to the measurement side of the force balance. Forces acting on the penetration in addition to those on the fin are therefore measured. The components other than lift, drag and pitching moment have been neglected as a result of this. A tare correction has not been made to the drag measurement for the skin friction acting on the circular penetration. Force balance outputs were recorded at 4 kHz and averaged over 4 seconds. The forces and moments are non-dimensionalised to give coefficients of lift, drag and pitching moment (measured about the base mid-chord) defined by $C_L = L/\frac{1}{2}\rho U^2 A$, $C_D = D/\frac{1}{2}\rho U^2 A$ and $C_M = M/\frac{1}{2}\rho U^2 Ac$ where L, D, and M are the lift, drag and pitching moment respectively, A the reference area (in this case the planform area of the fin) and ρ the fluid density.

On-body flow visualisation was achieved by oil flow tests using a mixture of titanium dioxide powder and silicone oil. Considerable experience has been gained in this technique from a range of experiments as to the quantity of titanium dioxide and viscosity of silicone oil required. A Typical mixture has a 1/10 ratio of titanium dioxide powder to silicone oil by mass. Silicone oils used have kinematic viscosities of 10, 100, 200, 500, 1000 and 5000 centiStokes depending on the shear stress involved. For the present experiments the 500 centiStoke kinematic viscosity oil was used. Tests were performed with the oil initially uniformly distributed for each incidence; the flow was then rapidly accelerated to the test velocity and the surface pattern allowed to reach equilibrium.

Off-body flow visualisation was by air injection via a reverse Pitot tube located 0.85m upstream of the fin location inserted varying depths into the flow depending upon the features to be visualised. Provided the bubbles are sufficiently small in diameter they are effective for flow visualisation or flow tracking. A procedure for calculating relative bubble velocities based on bubble size, length scales and velocity is given by Brennan [3]. Small bubbles can be produced using a reverse Pitot tube provided its internal diameter is small (in this case approximately 0.3mm) and there is some turbulence present to promote break up of larger bubbles and minimise coalescence. The bubbles were illuminated using a 150W flood lamp and images recorded using a Nikon 300D 35mm SLR digital camera. Both on and off-body flow visualisations were performed at incidences of 4, 8, 12, 14, 16, 18, 20, 22 and 26° at R_n=$4x10^5$.

Results

Lift, Drag and Pitching Moment

The variation of C_L, C_D and C_M against α, with R_n a parameter, is shown in Figure 2. Of particular interest are significant parameters of foil performance including the zero lift incidence for setting of fin angles on the surfboard, any discernible influence of the sharp leading edge, the lift slope and how this compares with published data, maximum lift and the type of stall.

There is relatively little variation of the C_L and C_D curves with R_n except at R_n = $2x10^5$ apart from an expected monotonic reduction in maximum C_L with decreasing R_n. There is a greater scatter in the data for the latter curves that can largely be attributed to estimated errors of the order of 10% at the lowest velocity. However, the break in the lift curve at around α=12 to 14° is characteristic of thin aerofoil stall behaviour associated with bursting of a laminar separation bubble at an intermediate incidence. The zero lift incidence is essentially invariant with R_n in the range tested at approximately -3.5°, indicating that fin

angles can be set regardless of anticipated velocity. The lift curve slope is also essentially invariant with R_n and is approximately 0.05/° which compares closely with the classical data compiled by Hoerner [5] for an aspect ratio of 3 and reduced for sweep as indicated in [5]. The maximum C_L varies approximately linearly with R_n and again compares closely with compiled data in [5] based on thickness and various aspect ratios. The lift curve peak is well rounded in all cases. The presence of a relatively small leading edge radius does not appear to have any deleterious effects on the fin performance. Measurements of both increasing and decreasing incidence showed essentially no effects of hysteresis or instability despite the complex nature of the flows involved.

Off-body Flow Visualisation

Results of off-body flow visualisations are presented in Figure 3 for 8, 12, 16 and 20° incidences at R_n = 4x10^5. The general flow pattern is dominated by the induced effect of the trailing tip vortex. At α=4° (Figure 3a) the inward and outward deflection of streamlines on the suction and pressure sides respectively can be clearly seen with the tip vortex core just becoming visible. Greater spanwise deflection of the streamlines is apparent at α=8° (Figure 3b) with the tip vortex core clearly evident. At α=12° (Figure 3c) the origin of the vortex core moves on to the suction surface of the foil inward of the tip. A similar pattern is observed at α=16° (Figure 3d). At α=20° (Figure 3e) bulk separation begins with a globally vortical nature about a point at approximately 60% span. At higher incidences the flow becomes fully separated from the leading edge although the vortical nature of the flow remains about a point which moves toward the fin base as incidence increases.

On-body Flow Visualisation

Results of on-body flow visualisations are presented in Figure 4 for 8, 12, 16 and 20° incidences at R_n = 4x10^5. In contrast with the off-body visualisation the on-body visualisation indicates a general outward flow on the suction surface, driven by the pressure gradient associated with the foil sweep. At α=4° (Figure 4a) the suction surface flow is laminar to about 40% chord and transitions without any laminar separation.

At α=8° (Figure 4b) the prominent attachment line around 30% chord near the base indicates the presence of a laminar separation bubble over the forward part of the foil. The flow at this incidence is essentially 2-D, with the extent of laminar flow decreasing forwards toward the tip. The forward movement of the attachment line (and reduction in extent of laminar flow) near the base is due to interactions with the turbulent boundary layer on the tunnel wall. A greater deflection of the surface streamlines indicates the presence of a secondary flow vortex in this interaction region. The wall boundary layer interaction effects become progressively more pronounced as incidence increases (Figure 4(c) and (d)) and a localised region of trailing edge flow separation appears to develop at the base on the suction surface.

A discontinuity in the attachment line develops near the tip at α=12° (Figure 4(c)) that is consistent with the off-body visualisation in Figure 3(c). This indicates the appearance of a three-dimensional separation zone near the foil tip as the origin of the tip vortex moves inboard onto the suction surface. These effects become pronounced at α=16° (Figure 4(d)). At α=20° (Figure 4(e)) the surface visualisation exhibits a classical focus pattern associated with a spiral point of separation. This tip stall phenomenon, which causes shedding of a part-span vortex sheet, is well known on aircraft with swept wings as described by Lighthill [6]. In this case the separation line issues from a saddle point separation at a part-span position (clearly evident in Figure 4e). The stall mechanism is therefore a combination of developing tip stall and localised trailing edge stall due to secondary flow interactions near the base.

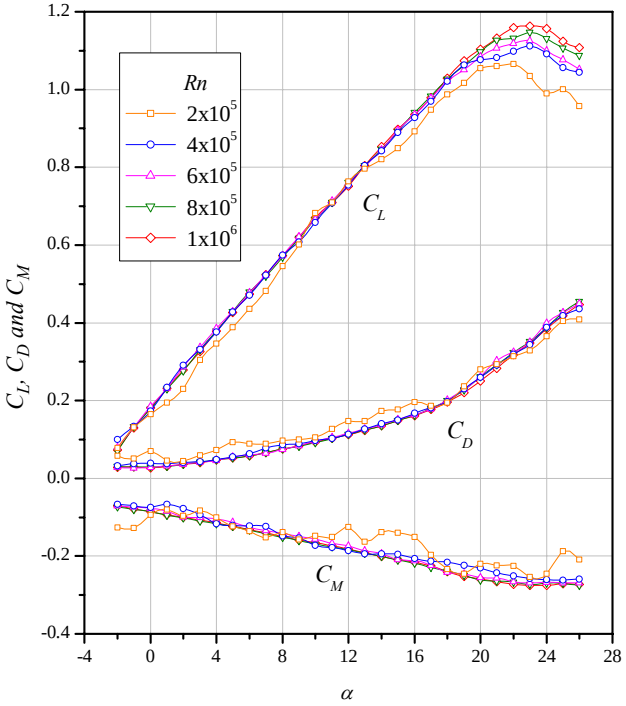

Figure 2. Lift, Drag and Pitching Moment Coefficients as a Function of Incidence with Reynolds Number a Parameter.

Conclusions

The hydrodynamic performance of a generic surfboard fin has been investigated. The measured forces and moments show relatively stable behaviour despite the presence of transitional flow with laminar separation at low Reynolds number. On and off-body flow visualisation reveal the extent of laminar flow and the influence of the wall boundary layer and tip vortex flow. These reveal that stall occurs as a combination of secondary flow effects at the base and three-dimensional stall at the foil tip.

Acknowledgments

The authors wish to acknowledge the assistance of Mr David Clarke in formulating the oil flow visualisation technique, Dr Colin Grubb and Mr Robert Wrigley for their assistance in carrying out experiments and the support of AMC, University of Tasmania, Surf Hardware International, Murray Burns & Dovell and the AusIndustry R&D Start Program.

References

[1] Brandner, P.A., *AMC Tom Fink Cavitation Tunnel – 6 Component Force Balance Laboratory Notes* , AMC, 2000.

[2] Brandner, P.A. and Walker G.J., *A Waterjet Test Loop for the Tom Fink Cavitation Tunnel*, International Conference on Waterjet Propulsion III, Royal Institution of Naval Architects, Gothenburg, Sweden, February, 2001, 54-57.

[3] Brennan, C.E., *Cavitation and Bubble Dynamics*, Oxford University Press, 1995.

[4] Hajime, Y., Hiroharu, K., Nobuhide., T, Hirofuml, S. and Masahiko, H., *Study on a Finite Span Foil with Sweptback Planform*, International Symposium on Cavitation: CAV95, Deauville, France, 1995, 367-372.

[5] Hoerner, S.F., *Fluid-Dynamic Lift*, Hoerner Fluid Dynamics, 1985.

[6] Lighthill, M.J., *Attachment and Separation in Three-dimensioanl Flow, Laminar Boundary Layers , Ed. L. Rosenhead*, Oxford University Press, 1963, 72-82.

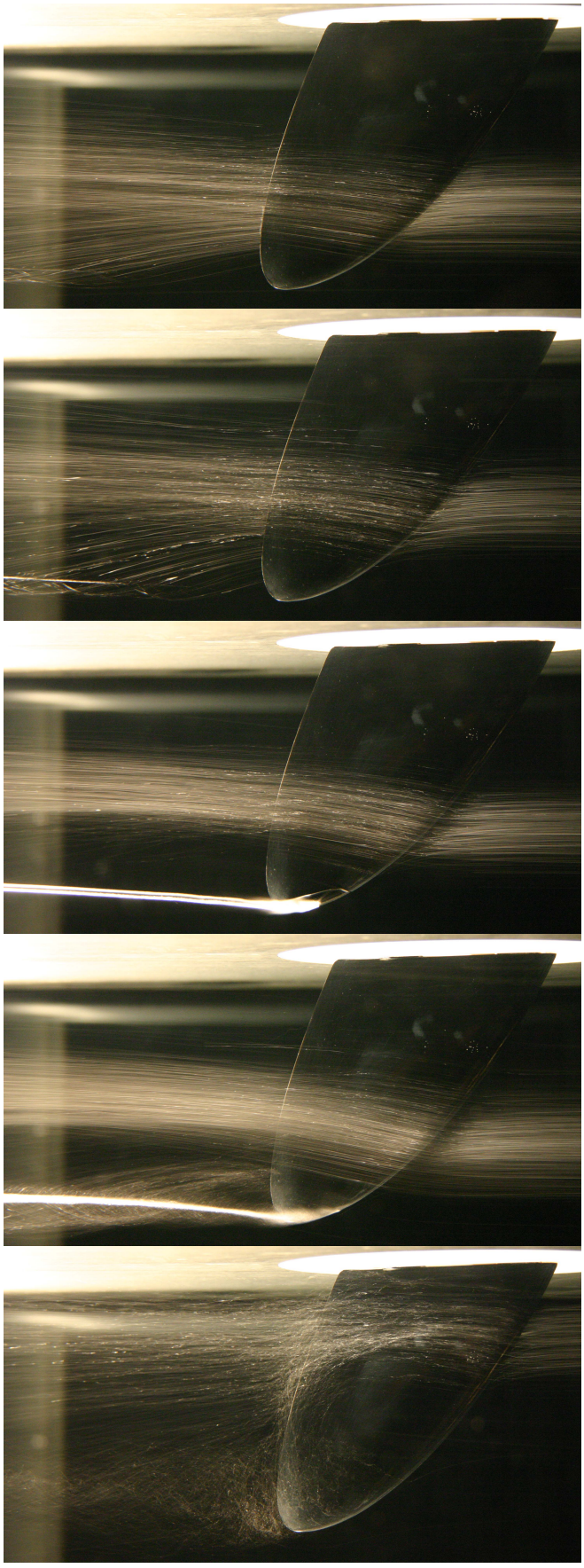

Figure 3. Off-body Flow Visualisation on the Suction Surface Using Air Injection at α = 4, 8, 12, 16 and 20° Incidence for R_n=4x10^5.

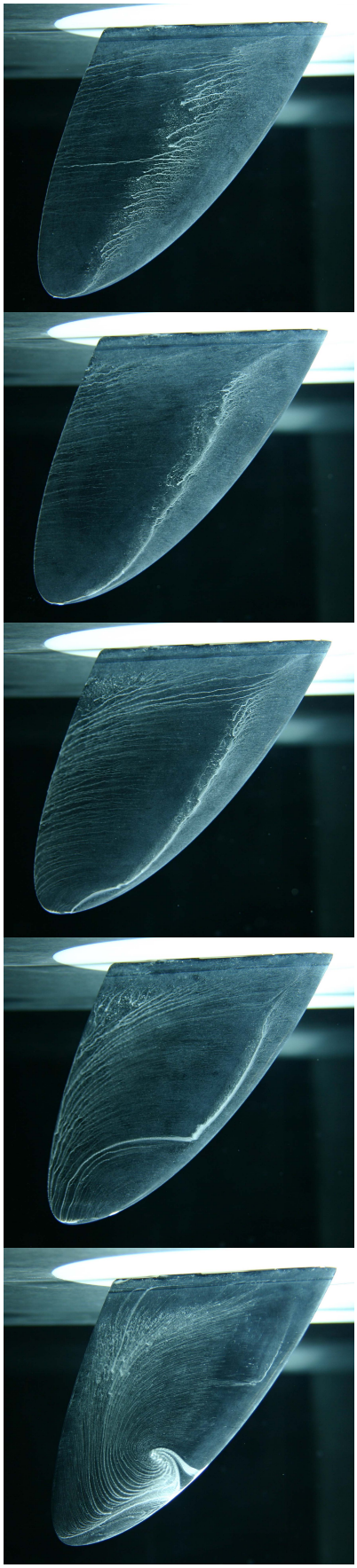

Figures 3a (Left) and 4a (Right) Off and On-body Flow Visualisation on the Suction Surface @ α=4°

Figures 3b (Left) and 4b (Right) Off and On-body Flow Visualisation on the Suction Surface @ α=8°

Figures 3c (Left) and 4c (Right) Off and On-body Flow Visualisation on the Suction Surface @ α=12°

Figures 3d (Left) and 4d (Right) Off and On-body Flow Visualisation on the Suction Surface @ α=16°

Figures 3e (Left) and 4e (Right) Off and On-body Flow Visualisation on the Suction Surface @ α=20°

Figure 4. On-body Flow Visualisation on the Suction Surface Using Oil Flow at α = 4, 8, 12, 16 and 20° Incidence for R_n=4x10^5.